J. KSIAM Vol.20, No.4, 309–332, 2016 http://dx.doi.org/10.12941/jksiam.2016.20.309

EFFECTS OF SORET AND DUFOUR ON NATURAL CONVECTIVE FLUID FLOW PAST A VERTICAL PLATE EMBEDDED IN POROUS MEDIUM IN PRESENCE OF THERMAL RADIATION VIA FEM

R. SRINIVASA RAJU

DEPARTMENT OF ENGINEERING, MATHEMATICS, GITAM UNIVERSITY, HYDERABAD CAMPUS, RUDRARAM, 502329, MEDAK (DT), TELANGANA, INDIA
E-mail address: srivass999@gmail.com

ABSTRACT. Finite element method has been applied to solve the fundamental governing equations of natural convective, electrically conducting, incompressible fluid flow past an infinite vertical plate surrounded by porous medium in presence of thermal radiation, viscous dissipation, Soret and Dufour effects. In this research work, the results of coupled partial differential equations are found numerically by applying finite element technique. The sway of significant parameters such as Soret number, Dufour number, Grashof number for heat and mass transfer, Magnetic field parameter, Thermal radiation parameter, Permeability parameter on velocity, temperature and concentration evaluations in the boundary layer region are examined in detail and the results are shown in graphically. Furthermore, the effect of these parameters on local skin friction coefficient, local Nusselt number and Sherwood numbers is also investigated. A very good agreement is noticed between the present results and previous published works in some limiting cases.

1. INTRODUCTION

1.1. **Literature Review of Natural Convection.** Natural convection flow encouraged by thermal and solutal buoyancy forces acting over bodies with different geometries in a fluid soaked porous medium is prevalent in many natural phenomena and has assorted and wide range of industrial applications. For example, in atmospheric flows, the occurrence of water or pure air is impossible because some foreign mass may be present either logically or mixed with air or water due to industrial productions. Natural processes such as vaporization of mist and fog, photosynthesis, drying of porous solids, reduction of toxic waste in water bodies, transpiration, sea-wind pattern (where upward convection is modified by Coriolis forces) and formation of ocean currents [1] happens due to thermal and solutal buoyancy forces urbanized as a result of difference in concentration or temperature or a combination of these two. Such configuration is also encountered in several practical systems for industry placed applications viz. cooling

Received by the editors July 11 2016; Revised November 30 2016; Accepted in revised form December 12 2016; Published online December 14 2016.

2000 *Mathematics Subject Classification.* 76W05, 76S05, 65L60.

Key words and phrases. Soret and Dufour, Viscous dissipation, Natural convection, Thermal radiation, Porous medium, Finite element method.

of molten metals, insulation systems, petroleum reservoirs, heat exchanger devices, chemical catalytic reactors, filtration and processes, nuclear waste repositories, desert coolers, frost formation in vertical channels, wet bulb thermometers etc. A numerical study was Garoosi et al. [2] carried out concerning natural and mixed convection heat transfer of nanofluid in a two-dimensional square cavity with numerous pairs of heat source-sinks. In this research, authors solved two-dimensional Navier–Stokes, energy and volume fraction equations by applying the finite volume method. Garoosi et al. [3] studied heat transfer natural convection of nanofluid in a two-dimensional square cavity containing numerous pairs of heater and coolers (HACs) using finite volume discretization method. Free convective heat and mass transfer in a steady two-dimensional magnetohydrodynamic fluid flow over a stretching vertical surface embedded in porous medium was studied by Rashidi et al. [4] using homotopy analysis method. The effect of non-uniform magnetic field on nanofluid forced convection heat transfer in a lid driven semi-annulus was discussed by Sheikholeslami et al. [5]. In this paper, authors used control volume based finite element method to solve the governing equations in the form of stream function-vorticity formulation for the thermophoresis and Brownian motion effects are taken into account. Rashidi et al. [6] studied the effect of magnetic field on natural convection surface boundary condition over a flat plate applying the one parameter group method. Rashidi et al. [7] discussed the natural convection flow of an incompressible third grade fluid between two parallel plates. In this paper, the governing equations of the flow were reduced to a set of nonlinear ordinary differential equations and the resulting nonlinear ordinary differential equations were solved by multi-step differential transform method. Heat transfer by simultaneous natural convection and radiation through an optically thick fluid over a heated vertical plate have been studied by Kang Cao and John Baker [8] with first-order momentum and thermal non-continuum boundary conditions. The influences of cooled auxiliary plate positions along the centerline of a vertical channel on combined natural convective in air and radiative heat transfer were investigated by Andreozzi and Man [9]. Adesanya et al. [10] investigated the free convective magneto hydrodynamic fluid flow through a channel with time periodic boundary condition with the effect of Joule dissipation.

1.2. **Literature Review of Viscous Dissipation.** The impact of viscous dissipation acting an important role in natural convective flows in various devices which are focused to large deceleration or which activate at high rotational speeds and also in strong gravitational field processes on large planets, geological processes and in nuclear engineering in association with the cooling of reactors. Fluid flow of natural convection is often encountered in cooling of nuclear reactors or in the study of the structure of stars and planets (Srinivasa Raju [11]). Great importance of temperature and heat transfer study has great importance to the engineers because of its almost universal happening in many branches of science and engineering. It is also essential to study the heat transfer from an asymmetrical surface because irregular surfaces are often nearby in many functions, such as radiator, heat exchangers and heat transfer enhancement devices. Sivaiah and Srinivasa Raju [11] studied the effect of Hall current on heat and mass transfer viscous dissipative fluid flow with heat source using finite element method. Ganga et al. [12] was investigated the effects of viscous and Ohmic dissipation on steady mathematically two-dimensional

radiative boundary-layer flow of a incompressible and electrically conducting nanofluid over a vertical plate internal heat generation/absorption. An unsteady, two-dimensional, hydromagnetic, laminar free convective boundary-layer flow of an electrically conducting, newtonian, incompressible and radiating fluid past an infinite heated vertical porous plate with heat and mass transfer was analyzed by Ramachandra Prasad and Bhaskar Reddy [13] taking into account the impact of viscous dissipation. The effect of radiation on two-dimensional free convective MHD flow of incompressible fluid occupied in a porous medium between two vertical wavy walls in presence of temperature dependent heat source was investigated by Dada and Disu [14]. In this research paper authors was assumed the flow consists of a mean part and a perturbed part. The resultant differential equations were solved by Differential Transform Method (DTM). The free convection heat with mass transfer for MHD non-Newtonian Eyring-Powell flow embedded in a porous medium, over an infinite vertical plate was studied by Eldabe [15] taking into account the effects of both viscous dissipation and heat source. Micropolar fluid behaviour on steady MHD mass transfer with free convection through a porous medium with constant heat and mass fluxes have been studied numerically by Haque et al. [16]. Pal and Talukdar [17] studied the effect of thermal radiation on an unsteady hydromagnetic convective heat and mass transfer for a viscous fluid past a semi-infinite vertical moving plate embedded in a porous media in the attendance of heat absorption and first-order chemical reaction of the species by using Perturbation technique. MHD boundary layer flow and heat transfer of a fluid with variable viscosity through a porous medium towards a stretching sheet by taking in to the effects of viscous dissipation in presence of heat source/sink was discussed by Dessie and Kishan [18]. Raju et al. [19] dealt with a steady MHD forced convective flow of a viscous fluid of finite depth in a saturated porous medium over a fixed horizontal channel with thermally insulated and impermeable bottom wall in the presence of viscous dissipation and joule heating. Reddy [20] studied the effects of thermal radiation, viscous dissipation, and Hall current effects on the hydromagnetic convection flow of an electrically conducting, viscous, incompressible fluid past over a stretching vertical flat plate.

1.3. **Literature Review of Soret and Dufour Effects.** When heat and mass transfer arise concurrently in a moving fluid, the relations between the fluxes and the motivating potentials are of a more come together nature. Hence an energy flux can be created not only by concentration gradients but also by temperature gradients. The energy flux caused by a concentration gradient is named the diffusion thermo (Dufour) effect. On the extra hand, mass fluxes can also be produced by temperature gradients and this signifies the thermal diffusion (Soret) effect. In the majority of the studies connected to heat and mass transfer processes, the effects of Soret and Dufour are disregarded on the basis that they are of a lesser order of magnitude than the effects showed by Fourier's and Fick's laws. The Soret effect, for example, has been employed for isotope separation and in mixture connecting gases with very light molecular weight (Hydrogen or Helium) and of medium molecular weight (Nitrogen or Air). The Dufour effect was established to be of order of extensively magnitude such that it cannot be unnoticed (Eckeret and Drake [21]). Rashidi et al. [22] investigated the combined effects viscous dissipation and Ohmic heating on steady MHD convective and slip flow due to a rotating disk

in presence of thermal diffusion and diffusion thermo via HAM. Sheri and Raju [23] studied the influence of Soret on an unsteady magnetohydrodynamics free convective flow past a semi-infinite vertical plate in the presence viscous dissipation. The results of thermal radiation and heat source on an unsteady MHD free convective fluid flow over an infinite vertical plate in occurrence of thermal-diffusion and diffusion-thermo were discussed by Raju et al. [24]. Rashidi and Erfani [25] studied the effects of thermal-diffusion and diffusion-thermo on combined heat and mass transfer of a steady magnetohydrodynamic convective and slip flow due to a rotating disk with viscous dissipation and Ohmic heating. The homotopy analysis method with two auxiliary parameters was employed by Rashidi et al. [26] to examined the effects of Soret and Dufour on a steady two-dimensional magnetohydrodynamic viscoelastic fluid flow over a stretching vertical surface in presence of heat and mass transfer. The effects of Soret and Dufour effects with heat and mass transfer on the steady, laminar mixed convection flow along a semi-infinite vertical plate surrounded in a micropolar fluid snowed under non-Darcy porous medium in presence of heat and mass flux conditions were investigated by Srinivasacharya and RamReddy [27]. Double-diffusive natural convection with Soret and Dufour effects in a square cavity filled with non-Newtonian power-law fluid has been simulated by finite difference Lattice Boltzmann method while entropy generations through fluid friction, heat transfer, and mass transfer were analyzed by Kefayati [28].

Based the above study, it can be said that, the Dufour and Soret effects on unsteady MHD free convective heat and mass transfer past an infinite vertical plate entrenched in a porous medium in the presence of thermal radiation. Hence, the purpose of this paper is to extend Prasad and Reddy [13] to study the more general problem which contains thermal radiation, Soret and Dufour on unsteady magnetohydrodynamic free convective flow past an infinite vertical plate. The momentum, thermal and solutal boundary layer governing equations are changed into a set of partial differential equations and then solved using finite element technique. The effects of a variety of governing parameters on the velocity, temperature, and concentration profiles including local Nusselt number and local Sherwood number are presented graphically and the local skin-friction coefficient in tabular form.

2. Mathematical formulation

Unsteady flow of a radiating, incompressible, viscous fluid flow past an infinite vertical plate entrenched in porous medium with time-dependent suction in an optically thin environment in presence of viscous dissipation is considered. The physical representation and the coordinate system is shown in Fig. 1. For this investigation, the following assumptions are made:

(1) The x'-axis is taken beside the vertical infinite plate embedded in porous medium in the upward direction and the y'-axis normal to the plate.
(2) At time $t' = 0$, the plate is preserved at a temperature T'_w, which is high enough to instigate radiative heat transfer.
(3) A stable magnetic field $H_o^{'2}$ is sustained in the y'-direction and the plate moves homogeneously along the positive x'-direction with velocity U_0.

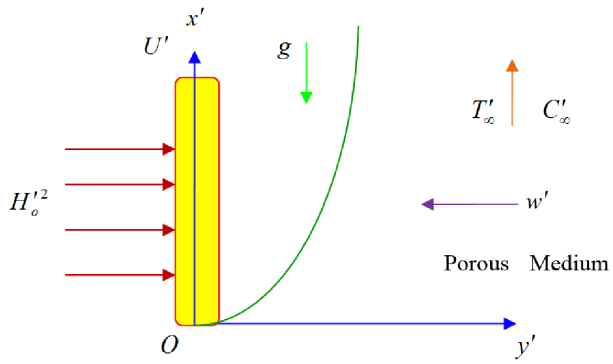

FIGURE 1. The physical representation and coordinate system of the problem.

(4) The fluid is supposed to be a slight conducting and hence the magnetic Reynolds number is lesser than unity and the induced magnetic field is small in comparison with the transverse magnetic field.
(5) It is further supposed that there is no applied voltage, as the electric field is absent.

Boussinesq's approximation the flow is reserved under the above assumptions by the following equations (Prasad and Reddy [13]):

Equation of continuity

$$\frac{\partial w'}{\partial y'} = 0 \tag{2.1}$$

Momentum equation

$$\left[\frac{\partial u'}{\partial t'}\right] + w'\left[\frac{\partial u'}{\partial y'}\right] = \nu\left[\frac{\partial^2 u'}{\partial y'^2}\right] - \left[\frac{\mu_e^2 \sigma_C H_0'^2}{\rho}\right](u' - U') - \left[\frac{\nu}{K'}\right](u' - U') + g\beta\,(T' - T'_\infty) + g\beta^*\,(C' - C'_\infty) + \frac{\partial U'}{\partial t'} \tag{2.2}$$

Energy equation

$$\left[\frac{\partial T'}{\partial t'}\right] + w'\left[\frac{\partial T'}{\partial y'}\right] = \frac{\kappa}{\rho c_P}\left[\frac{\partial^2 T'}{\partial y'^2}\right] - \frac{1}{\rho c_P}\left[\frac{\partial q'}{\partial y'}\right] + \frac{\nu}{c_P}\left[\left(\frac{\partial u'}{\partial y'}\right)^2\right] + \frac{D_m k_T}{c_S c_P}\left[\frac{\partial^2 C'}{\partial y'^2}\right] \tag{2.3}$$

Equation of radiative heat flux

$$\frac{\partial^2 q'}{\partial y'^2} - 3\alpha^2 q' - 16\alpha\,\sigma^*\,T_\infty'^3\frac{\partial T'}{\partial y'} = 0 \tag{2.4}$$

Species diffusion equation

$$\left[\frac{\partial C'}{\partial t'}\right] + w'\left[\frac{\partial C'}{\partial y'}\right] = D\left[\frac{\partial^2 C'}{\partial y'^2}\right] + \frac{D_m k_T}{T_m}\left[\frac{\partial^2 T'}{\partial y'^2}\right] \tag{2.5}$$

The corresponding boundary conditions are

$$\left.\begin{array}{l} t' \le 0: \quad u' = 0,\ T' = T'_\infty,\ C' = C'_\infty \ for\ \text{all}\ y' \\ t' > 0: \left\{ \begin{array}{l} u' = 0,\ T' = T'_w,\ C' = C'_w \ \text{at}\ y' = 0 \\ u' = U'(t') = w'_0\left(1 + \varepsilon\, e^{i\omega' t'}\right),\ T' \to T'_\infty,\ C' \to C'_\infty \ \text{as}\ y' \to \infty \end{array} \right. \end{array}\right\} \quad (2.6)$$

Since the fluid is optically thin with a moderately low density and α (absorption coefficient) $<< 1$, the radiative heat flux given by equation (2.4) in the strength of Cogley et al. [29] becomes

$$\frac{\partial q'}{\partial y'} = 4\alpha^2\left(T' - T'_\infty\right) \quad (2.7)$$

where $\alpha^2 = \displaystyle\int_0^\infty K_{\lambda w}\left(\frac{\partial B}{\partial T'}\right) d\lambda$.

Further, from Eq. (2.1) it is clear that w' is a constant or a function of time only and so we assume

$$w' = -w'_0\left(1 + \varepsilon A e^{\omega' t'}\right) \quad (2.8)$$

Such that $\varepsilon A \ll 1$, and the negative sign designates that the suction velocity is towards the plate. In order to write the governing equations and the boundary conditions in non-dimensional form, the following non-dimensional quantities are introduced:

$$\left.\begin{array}{l} y = \dfrac{w'_0 y'}{\nu},\ \omega = \dfrac{4\nu\omega'}{w'^2_0},\ t = \dfrac{w'^2_0 t'}{4\nu},\ u = \dfrac{u'}{U_0},\ U = \dfrac{U'}{U_0},\ \theta = \dfrac{T' - T'_\infty}{T'_w - T'_\infty}, \\ \mathrm{Pr} = \dfrac{\rho\nu c_p}{\kappa},\ Gr = \dfrac{g\beta\nu\left(T'_w - T'_\infty\right)}{U_0 w'^2_0},\ Gc = \dfrac{g\beta^*\nu\left(C'_w - C'_\infty\right)}{U_0 w'^2_0},\ R^2 = \dfrac{\nu 4\alpha^2}{\rho c_P w'^2_0}, \\ M^2 = \dfrac{\nu\mu_e^2\sigma_C H'^2_0}{\rho w'^2_0},\ \chi^2 = \dfrac{\nu^2}{K' w'^2_0},\ Sr = \dfrac{D_m k_T\left(T'_w - T'_\infty\right)}{\nu T_m\left(C'_w - C'_\infty\right)}, \\ Sc = \dfrac{\nu}{D},\ Ec = \dfrac{U_o^2}{c_P\left(T'_w - T'_\infty\right)},\ Du = \dfrac{D_m k_T\left(C'_w - C'_\infty\right)}{\nu c_S c_P\left(T'_w - T'_\infty\right)},\ \varphi = \dfrac{C' - C'_\infty}{C'_w - C'_\infty} \end{array}\right\} \quad (2.9)$$

In view of Eqs. (2.7), (2.8) and (2.9), Eqs. (2.2), (2.3) and (2.5) reduce to the following non-dimensional form

Momentum equation

$$\frac{1}{4}\frac{\partial u}{\partial t} - \left(1 + \varepsilon A\, e^{\omega t}\right)\frac{\partial u}{\partial y} = \frac{1}{4}\frac{\partial U}{\partial t} + \frac{\partial^2 u}{\partial y^2} - (M^2 + \chi^2)(u - U) + Gr\theta + Gc\varphi \quad (2.10)$$

Energy equation

$$\frac{1}{4}\frac{\partial \theta}{\partial t} - \left(1 + \varepsilon A\, e^{\omega t}\right)\frac{\partial \theta}{\partial y} = \frac{1}{\mathrm{Pr}}\left(\frac{\partial^2\theta}{\partial y^2} - R^2\right) + (Du)\left(\frac{\partial^2\varphi}{\partial y^2}\right) + (Ec)\left(\frac{\partial u}{\partial y}\right)^2 \quad (2.11)$$

Species diffusion equation

$$\frac{1}{4}\frac{\partial \varphi}{\partial t} - \left(1 + \varepsilon A\, e^{\omega t}\right)\frac{\partial \varphi}{\partial y} = \frac{1}{Sc}\frac{\partial^2\varphi}{\partial y^2} + (Sr)\left(\frac{\partial^2\theta}{\partial y^2}\right) \quad (2.12)$$

Equations (2.10), (2.11) and (2.12) are now subject to the boundary conditions

$$\left.\begin{array}{ll} t \le 0: & u = 0,\ \theta = 0,\ \varphi = 0 \text{ for all } y \\ t > 0: & \left\{\begin{array}{l} u = 0,\ \theta = 1,\ \varphi = 1 \text{ on } y = 0 \\ u \to 1 + \varepsilon e^{\omega t},\ \theta \to 0,\ \varphi \to 0 \text{ as } y \to \infty \end{array}\right. \end{array}\right\} \tag{2.13}$$

The mathematical statement of the problem is now complete and embodies the solution of Eqs. (2.10), (2.11) and (2.12) focus to boundary conditions (2.13). The skin-friction, Nusselt number and Sherwood number are important material parameters for this type of boundary layer flow. The skin-friction at the plate, which in the non-dimensional form is given by

$$C_f = \frac{\tau'_w}{\rho U_o \nu} = \left(\frac{\partial u}{\partial y}\right)_{y=0} \tag{2.14}$$

The rate of heat transfer coefficient, which in the non-dimensional form in terms of the Nusselt number is given by

$$Nu = -x\frac{\left(\frac{\partial T'}{\partial y'}\right)_{y'=0}}{T'_w - T'_\infty} \Rightarrow Nu\, Re_x^{-1} = -\left(\frac{\partial \theta}{\partial y}\right)_{y=0} \tag{2.15}$$

The rate of mass transfer coefficient, which in the non-dimensional form in terms of the Sherwood number, is given by

$$Sh = -x\frac{\left(\frac{\partial C'}{\partial y'}\right)_{y'=0}}{C'_w - C'_\infty} \Rightarrow Sh\, Re_x^{-1} = -\left(\frac{\partial \varphi}{\partial y}\right)_{y=0} \tag{2.16}$$

where $Re_x = U_o x/\nu$ is the local Reynolds number.

3. Numerical Solution by Finite Element Technique & Study of Grid Independence

3.1. **Finite Element Technique.** The finite element procedure (FEM) is a numerical and computer based method of solving a collection of practical engineering problems that happen in different fields such as, in heat transfer, fluid mechanics [30], chemical processing [31], rigid body dynamics [32], solid mechanics [33], and many other fields. It is recognized by developers and consumers as one of the most influential numerical analysis tools ever devised to analyze complex problems of engineering. The superiority of the method, its accuracy, simplicity, and computability all make it a widely used apparatus in the engineering modeling and design process. It has been applied to a number of substantial mathematical models, whose differential equations are solved by converting them into a matrix equation. The primary feature of FEM ([34] and [35]) is its ability to describe the geometry or the media of the problem being analyzed with huge flexibility. This is because the discretization of the region of the problem is performed using highly flexible uniform or non uniform pieces or elements that can easily describe complex shapes. The method essentially consists in assuming the piecewise continuous function for the results and getting the parameters of the functions in a manner that reduces the fault in the solution. The steps occupied in the finite element analysis areas follows.

Step 1: Discretization of the Domain: The fundamental concept of the FEM is to divide the region of the problem into small connected pieces, called finite elements. The group of elements is called the finite element mesh. These finite elements are associated in a non overlapping manner, such that they completely cover the entire space of the problem.

Step 2: Invention of the Element Equations:

(1) A representative element is secluded from the mesh and the variational formulation of the given problem is created over the typical element.
(2) Over an element, an approximate solution of the variational problem is invented, and by surrogating this in the system, the element equations are generated.
(3) The element matrix, which is also known as stiffness matrix, is erected by using the element interpolation functions.

Step 3: Assembly of the Element Equations: The algebraic equations so achieved are assembled by imposing the inter element continuity conditions. This yields a large number of mathematical equations known as the global finite element model, which governs the whole domain.

Step 4: Imposition of the Boundary Conditions: On the accumulated equations, the Dirichlet and Neumann boundary conditions (2.13) are imposed.

Step 5: Solution of Assembled Equations: The assembled equations so obtained can be solved by any of the numerical methods, namely, Gauss elimination technique, LU decomposition technique, and the final matrix equation can be solved by iterative technique. For computational purposes, the coordinate y is varied from 0 to $y_{\max} = 10$, where $y_{\max}$ represents infinity i.e., external to the momentum, energy and concentration edge layers.

3.2. **Variational formulation.** The variational formulation connected with Eqs. (2.10)-(2.12) over a typical two-nodded linear element $(y_e,\ y_{e+1})$ is given by

$$\int_{y_e}^{y_{e+1}} w_1 \left[\frac{\partial u}{\partial t} - B\frac{\partial u}{\partial y} - \frac{\partial U}{\partial t} - 4\frac{\partial^2 u}{\partial y^2} - 4(Gr)\theta - 4(Gc)\varphi - N\,(U-u)\right] dy = 0 \quad (3.1)$$

$$\int_{y_e}^{y_{e+1}} w_2 \left[\frac{\partial \theta}{\partial t} - B\frac{\partial \theta}{\partial y} - \frac{4}{\Pr}\frac{\partial^2 \theta}{\partial y^2} + \frac{4}{\Pr}R^2 - 4Du\frac{\partial^2 \varphi}{\partial y^2} - 4Ec\frac{\partial u}{\partial y}^2\right] dy = 0 \quad (3.2)$$

$$\int_{y_e}^{y_{e+1}} w_3 \left[\frac{\partial \varphi}{\partial t} - B\frac{\partial \varphi}{\partial y} - \frac{4}{Sc}\frac{\partial^2 \varphi}{\partial y^2} - 4Sr\frac{\partial^2 \theta}{\partial y^2}\right] dy = 0 \quad (3.3)$$

where $B = 4\left(1+\varepsilon A e^{nt}\right)$, $N = 4\left(M^2+\chi^2\right)$ and w_1, w_2, w_3 are arbitrary test functions and may be viewed as the variation in $u,\ \theta$ and φ respectively. After dropping the order of integration and non-linearity, we appear at the following system of equations.

$$\int_{y_e}^{y_{e+1}} \left[\begin{array}{l} (w_1)\left(\frac{\partial u}{\partial t}\right) - B\,(w_1)\left(\frac{\partial u}{\partial y}\right) + 4\left(\frac{\partial w_1}{\partial y}\right)\left(\frac{\partial u}{\partial y}\right) + N\,(w_1)\,u - 4\,(Gr)\,(w_1)\,\theta \\ -4\,(Gc)\,(w_1)\,\varphi - N\,(w_1)\,U - \frac{\partial U}{\partial t}\,(w_1) \end{array}\right] dy$$
$$- \left[4\,(w_1)\left(\frac{\partial u}{\partial y}\right)\right]_{y_e}^{y_{e+1}} = 0 \quad (3.4)$$

$$\int_{y_e}^{y_{e+1}} \left[\begin{array}{l} (w_2)\left(\frac{\partial\theta}{\partial t}\right) - B\,(w_2)\left(\frac{\partial\theta}{\partial y}\right) + \frac{4}{\mathrm{Pr}}\left(\frac{\partial w_2}{\partial y}\right)\left(\frac{\partial\theta}{\partial y}\right) + \frac{4}{\mathrm{Pr}}\,(w_2)\,R^2 \\ -4\,(Du)\,(w_2)\left(\frac{\partial w_2}{\partial y}\right)\left(\frac{\partial\varphi}{\partial y}\right) - 4\,(Ec)\,(w_2)\left(\frac{\partial\bar{u}}{\partial y}\right)\left(\frac{\partial u}{\partial y}\right) \end{array} \right] dy$$
$$- \left[4\left(\frac{w_2}{\mathrm{Pr}}\right)\left(\frac{\partial\theta}{\partial y}\right) - 4\,(Du)\,(w_2)\left(\frac{\partial\varphi}{\partial y}\right)\right]_{y_e}^{y_{e+1}} = 0 \tag{3.5}$$

$$\int_{y_e}^{y_{e+1}} \left[(w_3)\left(\frac{\partial\varphi}{\partial t}\right) - B\,(w_3)\left(\frac{\partial\varphi}{\partial y}\right) + \frac{4}{Sc}\left(\frac{\partial w_3}{\partial y}\right)\left(\frac{\partial\varphi}{\partial y}\right) - 4\,(Sr)\left(\frac{\partial w_3}{\partial y}\right)\left(\frac{\partial\varphi}{\partial y}\right)\right] dy$$
$$- \left[4\left(\frac{w_3}{Sc}\right)\left(\frac{\partial\varphi}{\partial y}\right) - 4\,(Sr)\,(w_3)\left(\frac{\partial\varphi}{\partial y}\right)\right]_{y_e}^{y_{e+1}} = 0 \tag{3.6}$$

3.3. **Finite Element formulation.** The finite element model may be obtained from Eqs. (3.4)-(3.6) by replacing finite element approximations of the form:

$$u = \sum_{j=1}^{2} u_j^e \psi_j^e, \quad \theta = \sum_{j=1}^{2} \theta_j^e \psi_j^e, \quad \varphi = \sum_{j=1}^{2} \varphi_j^e \psi_j^e \tag{3.7}$$

with $w_1 = w_2 = w_3 = \psi_j^e$ $(i = 1,\ 2)$, where $u_j^e,\ \theta_j^e$ and φ_j^e are the velocity, temperature and concentration respectively at the jth node of typical eth element $(y_e,\ y_{e+1})$ and ψ_i^e are the shape functions for this element $(y_e,\ y_{e+1})$ and are taken as:

$$\psi_1^e = \frac{y_{e+1} - y}{y_{e+1} - y_e} \text{ and } \psi_2^e = \frac{y - y_e}{y_{e+1} - y_e},\ y_e \le y \le y_{e+1} \tag{3.8}$$

The finite element model of the equations for eth element thus formed is given by

$$\left[\begin{array}{ccc} [K^{11}] & [K^{12}] & [K^{13}] \\ [K^{21}] & [K^{22}] & [K^{23}] \\ [K^{31}] & [K^{32}] & [K^{33}] \end{array}\right] \left[\begin{array}{c} \{u^e\} \\ \{\theta^e\} \\ \{\varphi^e\} \end{array}\right] + \left[\begin{array}{ccc} [M^{11}] & [M^{12}] & [M^{13}] \\ [M^{21}] & [M^{22}] & [M^{23}] \\ [M^{31}] & [M^{32}] & [M^{33}] \end{array}\right] \left[\begin{array}{c} \{u'^e\} \\ \{\theta'^e\} \\ \{\varphi'^e\} \end{array}\right] = \left[\begin{array}{c} \{b^{1e}\} \\ \{b^{2e}\} \\ \{b^{3e}\} \end{array}\right] \tag{3.9}$$

where $\{[K^{mn}],\ [M^{mn}]\}$ and $\{\{u^e\},\ \{\theta^e\},\ \{\varphi^e\},\ \{u'^e\},\ \{\theta'^e\},\ \{\varphi'^e\}$ and $\{b^{me}\}\ \}$ $(m,\ n = 1,\ 2,\ 3)$ are the set of matrices of order 2×2 and 2×1 respectively. These matrices are defined as follows

$$M_{ij}^{11} = \int_{y_e}^{y_{e+1}} (\psi_i^e)\,(\psi_j^e) dy,\ M_{ij}^{12} = M_{ij}^{13} = 0,$$

$$K_{ij}^{11} = -B \int_{y_e}^{y_{e+1}} \left[(\psi_i^e)\left(\frac{\partial\psi_j^e}{\partial y}\right)\right] dy + 4 \int_{y_e}^{y_{e+1}} \left[\left(\frac{\partial\psi_i^e}{\partial y}\right)\left(\frac{\partial\psi_j^e}{\partial y}\right)\right] dy,$$

$$K_{ij}^{12} = N \int_{y_e}^{y_{e+1}} \left[(\psi_i^e)\,(\psi_j^e)\right] dy - \left[N\,(U) + \left(\frac{\partial U}{\partial t}\right)\right] \int_{y_e}^{y_{e+1}} [\psi_i^e] dy,$$

$$K_{ij}^{13} = -4\,[Gr + Gc] \int_{y_e}^{y_{e+1}} (\psi_i^e)\,(\psi_j^e) dy,\ K_{ij}^{21} = -4\,(Ec) \int_{y_e}^{y_{e+1}} \left[(\psi_i^e)\left(\frac{\partial\bar{u}}{\partial y}\right)\left(\frac{\partial\psi_j^e}{\partial y}\right)\right] dy,$$

$$K_{ij}^{22} = -B\int_{y_e}^{y_{e+1}}\left[(\psi_i^e)\left(\frac{\partial\psi_j^e}{\partial y}\right)\right]dy + \frac{4}{\mathrm{Pr}}\int_{y_e}^{y_{e+1}}\left[\left(\frac{\partial\psi_i^e}{\partial y}\right)\left(\frac{\partial\psi_j^e}{\partial y}\right)\right]dy,$$

$$K_{ij}^{23} = \frac{4}{\mathrm{Pr}}R^2\int_{y_e}^{y_{e+1}}[\psi_i^e]dy - Du\int_{y_e}^{y_{e+1}}\left(\frac{\partial\psi_i^e}{\partial y}\right)\left(\frac{\partial\psi_j^e}{\partial y}\right)dy,\ M_{ij}^{21} = M_{ij}^{23} = 0,$$

$$M_{ij}^{22} = \int_{y_e}^{y_{e+1}}(\psi_i^e)\left(\psi_j^e\right)dy,\ M_{ij}^{31} = M_{ij}^{32} = 0,\ M_{ij}^{33} = \int_{y_e}^{y_{e+1}}(\psi_i^e)\left(\psi_j^e\right)dy,$$

$$K_{ij}^{31} = 0,\ K_{ij}^{32} = -4\,(Sr)\int_{y_e}^{y_{e+1}}\left(\frac{\partial\psi_i^e}{\partial y}\right)\left(\frac{\partial\psi_j^e}{\partial y}\right)dy,$$

$$K_{ij}^{33} = -B\int_{y_e}^{y_{e+1}}\left[(\psi_i^e)\left(\frac{\partial\psi_j^e}{\partial y}\right)\right]dy + \frac{4}{Sc}\int_{y_e}^{y_{e+1}}\left[\left(\frac{\partial\psi_i^e}{\partial y}\right)\left(\frac{\partial\psi_j^e}{\partial y}\right)\right]dy,$$

$$b_i^{1e} = 4\left[(\psi_i^e)\left(\frac{\partial\psi_j^e}{\partial y}\right)\right]_{y_e}^{y_{e+1}},\ b_i^{2e} = \left[4\left(\frac{\psi_i^e}{\mathrm{Pr}}\right)\left(\frac{\partial\psi_j^e}{\partial y}\right) - 4\,(Du)\,(\psi_i^e)\left(\frac{\partial\psi_j^e}{\partial y}\right)\right]_{y_e}^{y_{e+1}},$$

$$b_i^{3e} = \left[4\left(\frac{\psi_i^e}{Sc}\right)\left(\frac{\partial\psi_j^e}{\partial y}\right) - 4\,(Sr)\,(\psi_i^e)\left(\frac{\partial\psi_j^e}{\partial y}\right)\right]_{y_e}^{y_{e+1}}$$

In one-dimensional space, linear and quadratic elements, or element of higher order can be taken. The entire flow province is divided into 11000 quadratic elements of equal size. Each element is three-noded, and therefore the whole domain contains 21001 nodes. At each node, four functions are to be evaluated; hence, after assembly of the element equations, we acquire a system of 81004 equations which are nonlinear. Therefore, an iterative scheme must be developed in the solution. After striking the boundary conditions, a system of equations has been obtained which is solved mathematically by the Gauss elimination method while maintaining a correctness of 0.00001. A convergence criterion based on the relative difference between the present and preceding iterations is employed. When these differences satisfy the desired correctness, the solution is assumed to have been congregated and iterative process is terminated. The Gaussian quadrature is applied for solving the integrations. The computer cryptogram of the algorithm has been performed in MATLAB running on a PC. Excellent convergence was completed for all the results.

3.4. **Study of Grid Independence.** In general, to study the grid independency/dependency, how should the mesh size be varied in order to check the solution at different mesh (grid) sizes and get a range at which there is no variation in the solutions. We showed the numerical values of velocity (u), temperature (θ) and concentration (φ) for different values of mesh (grid) size at time $t = 1.0$ in the following table 1.

From this table 1, we observed that there is no variation in the values of velocity (u), temperature (θ) and concentration (φ) for different values of mesh (grid) size at time $t = 1.0$. Hence, we conclude that, the results are independent of mesh (grid) size.

TABLE 1. The numerical values of u, θ and ϕ for variation of mesh sizes at $t = 1.0$

Mesh (Grid) size$= 0.01$			Mesh (Grid) size$= 0.001$		
u	θ	φ	u	θ	φ
0.000000	1.000000	1.000000	0.000000	1.000000	1.000000
2.974329	0.369802	0.548479	2.974329	0.369802	0.548479
3.370421	0.169484	0.274438	3.370421	0.169484	0.274438
3.026220	0.081939	0.135010	3.026220	0.081939	0.135010
2.577752	0.040053	0.066201	2.577752	0.040053	0.066201
2.210582	0.019617	0.032440	2.210582	0.019617	0.032440
1.949927	0.009608	0.015892	1.949927	0.009608	0.015892
1.771644	0.004700	0.007776	1.771644	0.004700	0.007776
1.640400	0.002287	0.003788	1.640400	0.002287	0.003788
1.518096	0.001087	0.001806	1.518096	0.001087	0.001806
1.358957	0.000461	0.000777	1.358957	0.000461	0.000777
Mesh (Grid) size$= 0.0001$			Mesh (Grid) size$= 0.00001$		
u	θ	φ	u	θ	φ
0.000000	1.000000	1.000000	0.000000	1.000000	1.000000
2.974329	0.369802	0.548479	2.974329	0.369802	0.548479
3.370421	0.169484	0.274438	3.370421	0.169484	0.274438
3.026220	0.081939	0.135010	3.026220	0.081939	0.135010
2.577752	0.040053	0.066201	2.577752	0.040053	0.066201
2.210582	0.019617	0.032440	2.210582	0.019617	0.032440
1.949927	0.009608	0.015892	1.949927	0.009608	0.015892
1.771644	0.004700	0.007776	1.771644	0.004700	0.007776
1.640400	0.002287	0.003788	1.640400	0.002287	0.003788
1.518096	0.001087	0.001806	1.518096	0.001087	0.001806
1.358957	0.000461	0.000777	1.358957	0.000461	0.000777

4. PROGRAM VALIDATION AND COMPARISON WITH PREVIOUS RESEARCH

In order to check on the correctness of the numerical technique used for the solution of the problem considered in the present study, it was authenticated by performing simulation for numerical solutions for the effects of radiation and mass transfer on an unsteady magnetohydrodynamic free convective flow past a heated vertical plate embedded in a porous medium in presence of viscous dissipation which are reported by Prasad and Reddy [13]. Tables 2, 3, 4 and 5 show the calculated values for skin-friction, Rate of heat and mass transfer coefficients for the present solution when $Sr = Du = 0$, and the results in published by Prasad and Reddy [13]. Tables 2, 3, 4 and 5 show a very good concurrence between the results and this lends confidence to the present numerical code.

TABLE 2. Comparison between present skin-friction (C_f) and Nusselt number $(Nu\ Re_x^{-1})$ results with the results $(C_f^*,\ Nu^* Re_x^{-1})$ of Prasad and Reddy [13] for different values of Ec.

Ec	C_f	C_f^*	$Nu\ Re_x^{-1}$	$Nu^*\ Re_x^{-1}$
0.0	1.63024458	1.6302	3.33965172	3.3396
0.001	1.48365516	1.4836	3.09564923	3.0956
0.010	0.16443199	0.1644	0.89964186	0.8996

TABLE 3. Comparison between present skin-friction (C_f) and Nusselt number $(Nu\ Re_x^{-1})$ results with the results $(C_f^*,\ Nu^* Re_x^{-1})$ of Prasad and Reddy [13] for different values of R.

R	C_f	C_f^*	$Nu\ Re_x^{-1}$	$Nu^*\ Re_x^{-1}$
0.0	3.76701694	3.7670	0.67210943	0.6721
0.5	3.47752292	3.4775	1.10649216	1.1064
1.0	3.32915508	3.3291	1.35993044	1.3599
1.5	3.09568774	3.0956	1.48367628	1.4836

TABLE 4. Comparison between present skin-friction (C_f) and Sherwood number $(Sh\ Re_x^{-1})$ results with the results $(C_f^*,\ Sh^* Re_x^{-1})$ of Prasad and Reddy [13] for different values of Sc.

Sc	C_f	C_f^*	$Sh\ Re_x^{-1}$	$Sh^*\ Re_x^{-1}$
0.22	3.73162208	3.7316	0.22011848	0.2201
0.60	3.47751182	3.4775	0.60183321	0.6018
0.78	3.39804066	3.3980	0.78044923	0.7804
0.94	3.34001101	3.3400	0.94031584	0.9403

TABLE 5. Comparison between present skin-friction (C_f) results with the results (C_f^*) of Prasad and Reddy [13] for different values of Gr and Gc.

Gr	C_f	C_f^*	Gc	C_f	C_f^*
0	2.52780649	2.5278	0	2.80126472	2.8012
1	3.10972668	3.0197	1	3.47753994	3.4775
2	3.47751623	3.4775	2	4.14845591	4.1484
3	3.88681947	3.8868	3	4.81384067	4.8138

5. Discussion of the results

In the preceding sections, we have prepared and solved the problem of an unsteady MHD free convection flow past an infinite heated vertical plate surrounded in a porous medium with thermal-diffusion, diffusion-thermo, viscous dissipation and radiation. By interesting, the optically thin differential approximation for the radiative heat flux in the energy equation. In the numerical calculation, the Prandtl number ($Pr = 0.71$) which corresponds to air and different values of the stuff parameters are used. In addition, the boundary condition $y \to \infty$ is approximated by $y_{\max} = 10$, which is adequately large for the velocity to approach the appropriate stream velocity. The temperature and the species concentration are coupled to the velocity through Grashof number for heat and mass transfer as seen in Eq. (2.10). For assorted values of Grashof number for heat and mass transfer, the velocity profiles u are plotted in Figs. 2 (a) and 2 (b).

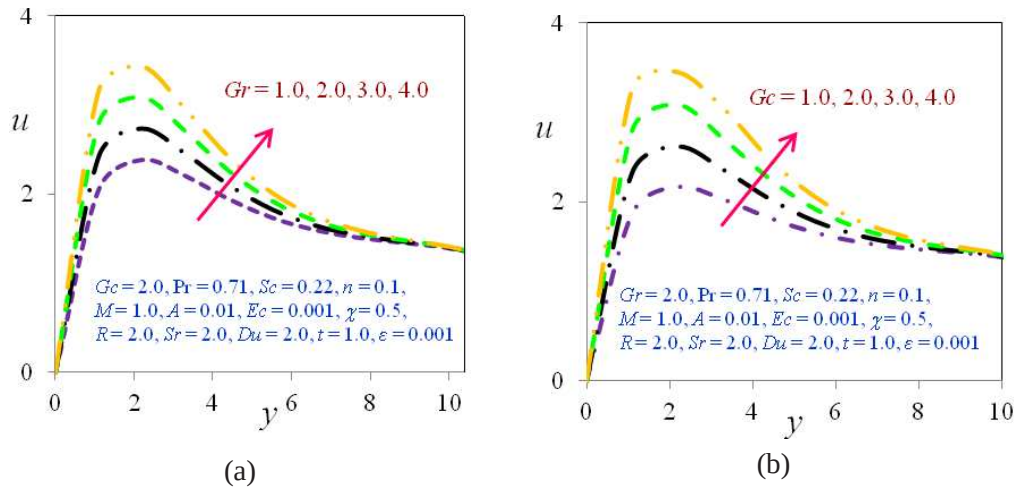

FIGURE 2. Effect of (a) *Gr* , (b) *Gc* on velocity profiles

The Grashof number for heat transfer indicates the relative effect of the thermal buoyancy force to the viscous hydrodynamic force in the boundary layer. As expected, it is observed that there is a increase in the velocity due to the enhancement of thermal buoyancy force. Also, as *Gr* raises, the peak values of the velocity increases quickly near the porous plate and then decomposes smoothly to the free stream velocity. The Grashof number for mass transfer characterizes the ratio of the buoyancy force to the viscous hydrodynamic force. As usual, the fluid velocity increases and the peak value is more distinctive due to enhance in the species buoyancy force. The velocity distribution reaches a distinctive greatest value in the locality of the plate and then decreases properly to move towards the free stream value. It is perceived that the velocity magnifies with increasing values of Grashof number for mass transfer.

Fig. 3 (a) demonstrates the velocity profiles for dissimilar values of Prandtl number Pr. The mathematical results show that the effect of growing values of Prandtl number result in

diminishing velocity. The nature of velocity profiles in presence of distant species such as *Sc* = 0.22 (Hydrogen), 0.30 (Helium), 0.60 (Oxygen) and 0.78 (Ammonia) are showing in Fig. 3 (b).

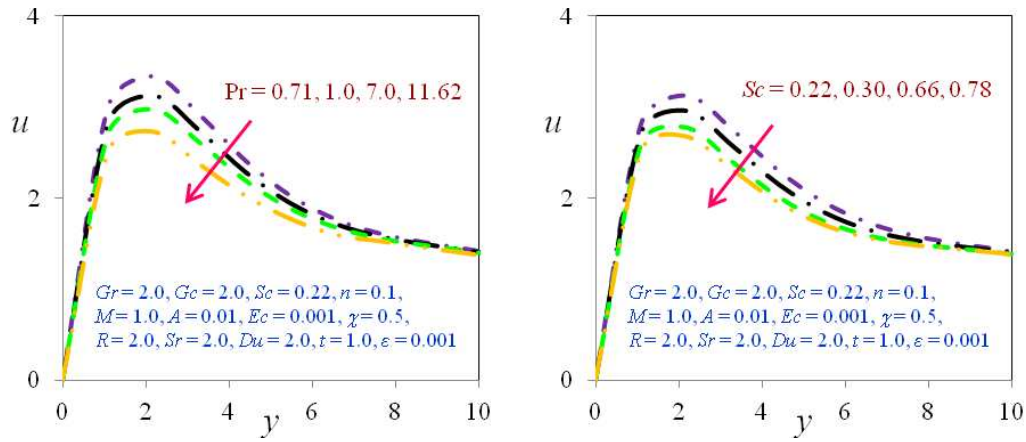

FIGURE 3. Effect of (a) Pr, (b) Sc on velocity profiles

The flow field experiences a decrease in velocity at all points in attendance of heavier diffusing species. The results of the magnetic field parameter M is shown in Fig. 4 (a).

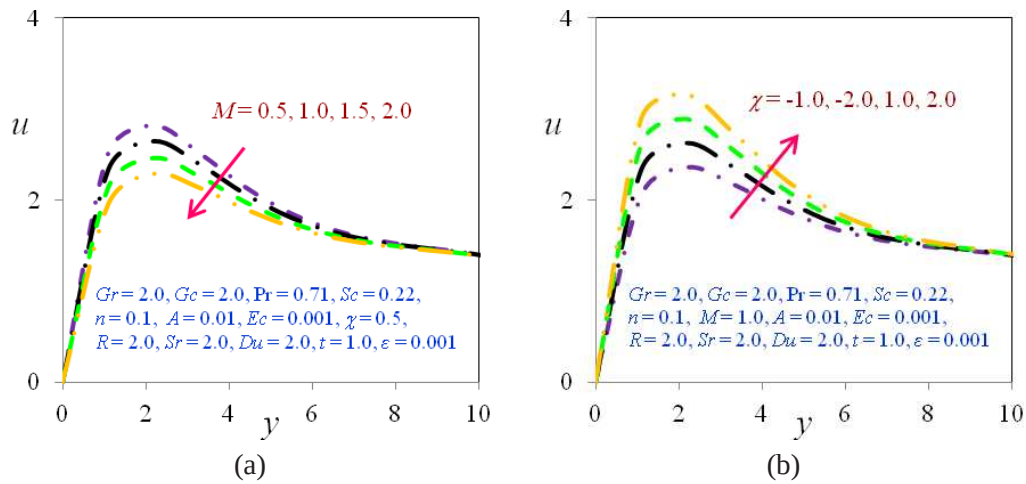

FIGURE 4. Effect of (a) M, (b) χ on velocity profiles

It is noticed that the velocity of the fluid diminishes with the raises of the magnetic field parameter values. The reduce in the velocity as the Hartmann number M increases is because the occurrence of a magnetic field in an electrically conducting fluid initiates a force called

the Lorentz force, which acts adjacent to the flow when the magnetic field is acted in the perpendicular direction, as in the present study. This resistive force deliberates down the fluid velocity component as shown in Fig. 4 (a). Fig. 4 (b) shows the effects of Darcy number χ on the velocity profiles for cooling as well as heating of the plate. For a cooling plate fluid velocity increases, while for a heating plate it decreases with increase of χ. Darcy number is the capacity of the porosity of the medium. With increasing porosity of the medium, the value of χ increases. For large porosity of the medium fluid acquires more space to flow as a consequence its velocity increases. The effect of the thermal radiation parameter R on the velocity and temperature profiles in the boundary layer are demonstrated in Figs. 5 (a) and 5 (b), respectively.

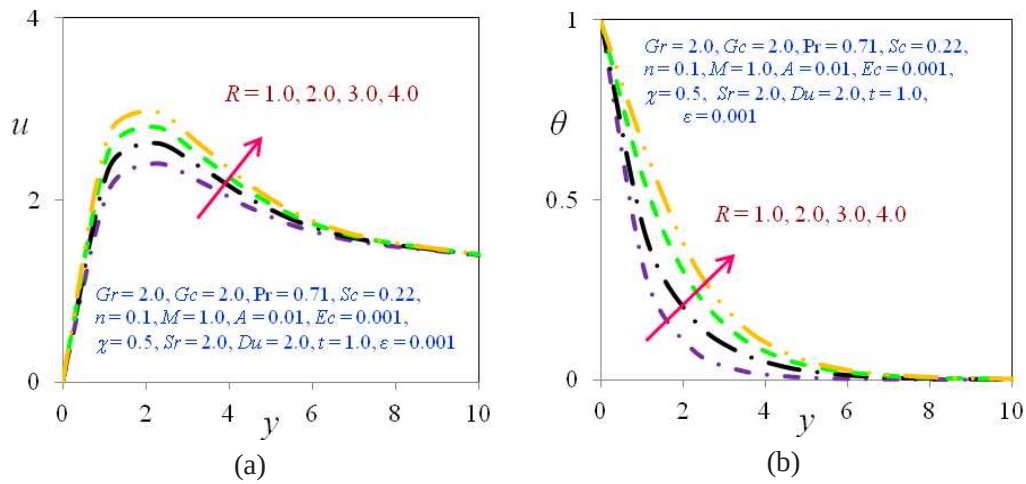

FIGURE 5. Effect of (a) R on velocity, (b) R on temperature profiles

With increasing the thermal radiation parameter Rconstructs significant boost in the thermal condition of the fluid and its thermal boundary layer. This increase in the fluid temperature brings more flow in the boundary layer reasoning the velocity of the fluid there to increase. The influence of the viscous dissipation (Eckert number) parameter on the velocity and temperature profiles are shown in Figs. 6 (a) and 6 (b), respectively.

The relationship between the kinetic energy in the flow and the enthalpy is given by Eckert number. It represents the exchange of kinetic energy into internal energy by work done against the viscous fluid stresses. Larger viscous dissipative heat causes a grow in the temperature as well as the velocity. This performance is evident from Figs. 6 (a) and 6 (b). Figs. 7 (a) and 7 (b) describe the velocity and concentration profiles for different values of the Soret (thermal diffusion) number.

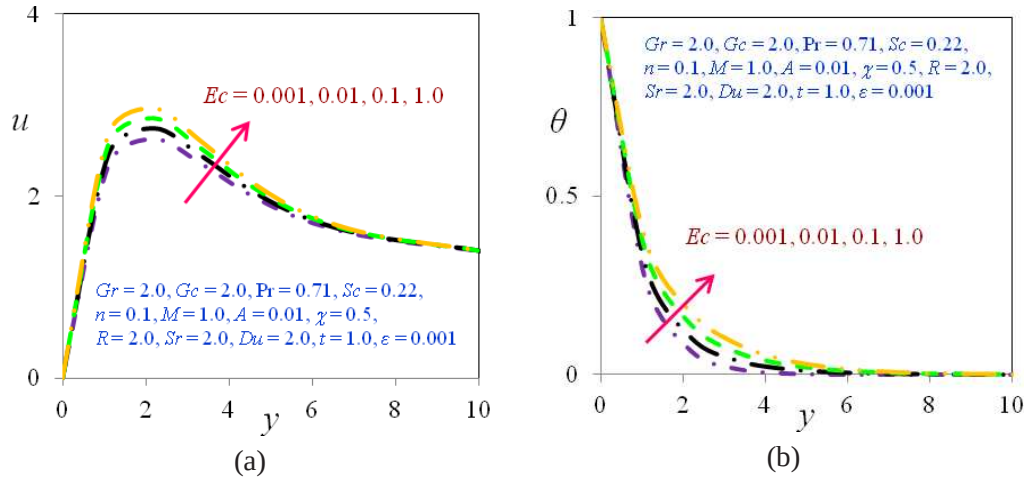

FIGURE 6. Effect of (a) *Ec* on velocity (b) *Ec* on temperature profiles

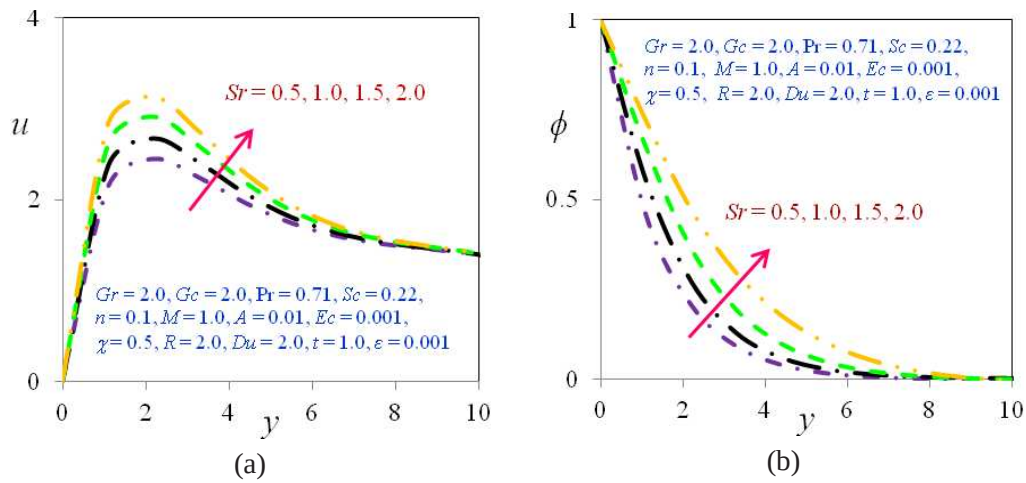

FIGURE 7. Effect of (a) *Sr* on velocity, (b) *Sr* on concentration profiles

The Soret number classifies the effect of the temperature gradients inducing significant mass diffusion effects. It is observed that an increase in the Soret number results in an increase in the velocity and concentration within the boundary layer. For different values of the Dufour (diffusion thermo) number, the velocity and temperature profiles are designed in Figs. 8 (a) and 8 (b), respectively.

The Dufour number signifies the contribution of the concentration gradients to the thermal energy flux in the flow. It is institutes that an increase in the Dufour number causes a rise in the velocity and temperature all over the boundary layer. For, the temperature profiles decompose

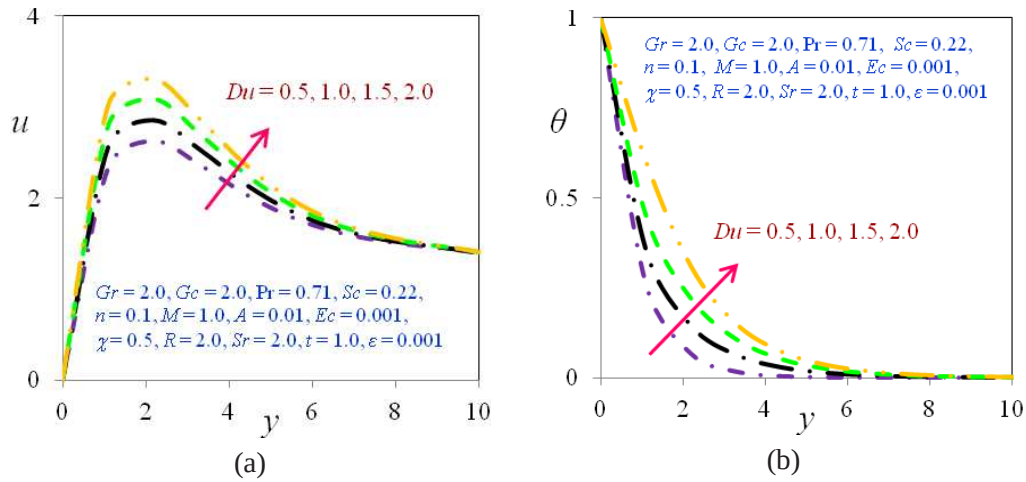

FIGURE 8. Effect of (a) *Du* on velocity, (b) *Du* on temperature profiles

smoothly from the plate to the free stream value. However for, a distinct velocity overshoot exists near the plate, and thereafter the profile falls to zero at the edge of the boundary layer.

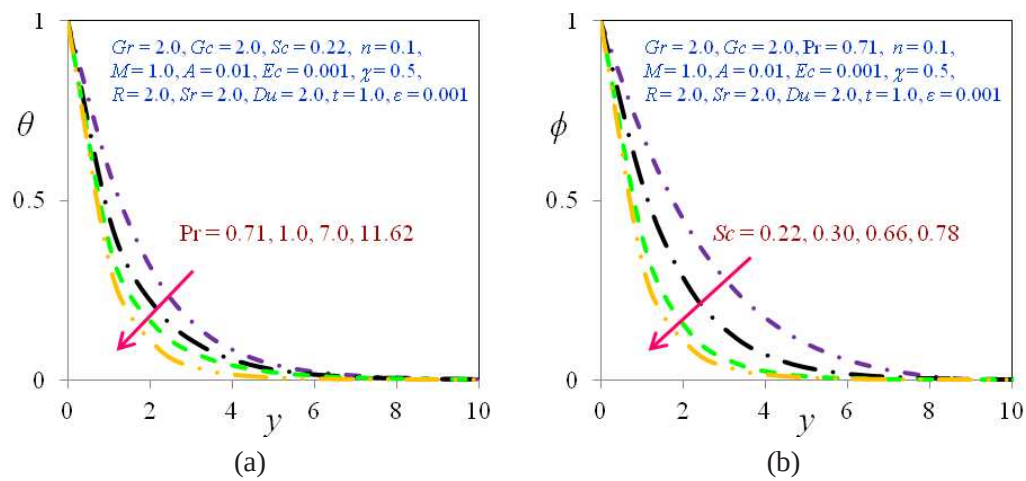

FIGURE 9. Effects of (a) Pr on temperature, (b) Sc on concentration profiles

Fig. 9 (a) illustrate the temperature profiles for dissimilar values of Prandtl number Pr. It is scrutinized that the temperature decrease as an increasing the Prandtl number. The reason is that smaller values of Pr are equivalent to amplify in the thermal conductivity of the fluid and then heat is able to diffuse away from the heated surface more quickly for higher values of Pr. Hence in the case of lesser Prandtl number the thermal boundary layer is substantial and the rate of heat transfer is reduced. Fig. 9 (b) shows the concentration field due to dissimilarities

in Schmidt number for the gasses Hydrogen, Helium, Oxygen and Ammonia. It is observed that concentration field is progressively for Hydrogen and drops rapidly for Oxygen and Ammonia in assessment to water-vapour. Thus Hydrogen can be used for preserving effective concentration field and water-vapour can be used for sustaining normal concentration field.

5.1. **Local skin-friction** (C_f)**.** The numerical values of local skin-friction are presented in table 6 for dissimilar values of Magnetic field (Hartmann number), Porosity parameter (Darcy number), Soret and Dufour numbers. It is observed from this table that

- The skin-friction increases from 2.95431478 to 3.26981158 with decreasing the value of M from 4.0 to 2.0, while reverse effect is found for χ (skin-friction decreases from 3.01140566 to 2.88523694 with increasing the value of χ from 2.0 to 3.0).
- The skin-friction increases as *Sr* increases from 1.0 to 2.0; thereafter however it increases with a succeeding value of *Sr* to 3.0 through to the least value of 1.0.
- Dufour number (*Du*) has towering impact on skin-friction. The skin-friction enhances from 3.26981158 to 3.46317524 with increasing the value of *Du* from 1.0 to 3.0.

TABLE 6. Variation of numerical values of skin-friction (C_f) for different values of M, *Sr*, *Du* and χ

M	χ	*Sr*	*Du*	C_f
2.0	1.0	1.0	1.0	3.26981158
4.0				2.95431478
6.0				2.61228304
	2.0			3.01140566
	3.0			2.88523694
		2.0		3.36951587
		3.0		3.45902413
			2.0	3.37683951
			3.0	3.46317524

5.2. **Local rate of heat transfer** $(Nu\ Re_x^{-1})$**.** The graphical results of local rate of heat transfer are presented in Figs. 10 (a), 10 (b) and 11 (a) for disparate values of Eckert number, Dufour number and thermal radiation parameter, respectively. It is observed from these figures that

- An increase in Dufour number gradually increases the magnitude of Nusselt number.
- The effectiveness of the thermal radiation parameter has lean impact on rate of heat transfer. i.e. the Nusselt number diminishes when increasing the thermal radiation parameter.
- Rate of heat transfer enhances with increasing of viscous dissipation (Eckert number) parameter.

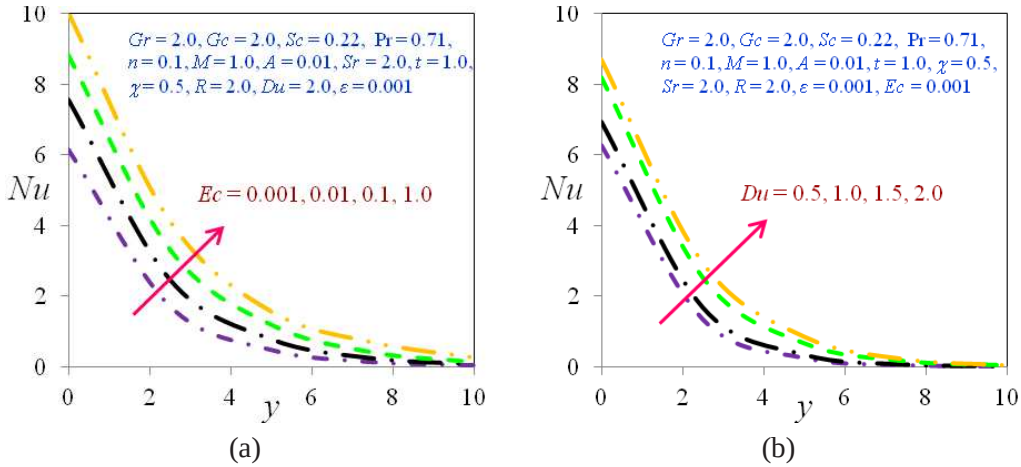

FIGURE 10. Effects of (a) *Ec* , (b) *Du* on rate of heat transfer

5.3. **Local rate of mass transfer** $(Sh\ Re_x^{-1})$**.** The results of local rate of mass transfer are presented in Fig. 11 (b) for changed values of Soret number. It is observed from this table that the effect of Soret number is seen more prominently for rate of mass transfer i.e., there is sharp increase in the value of rate of mass transfer.

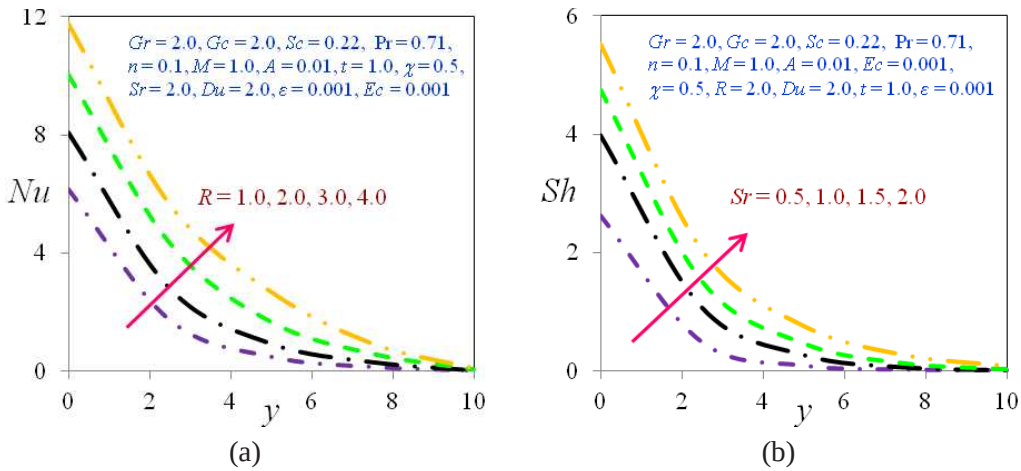

FIGURE 11. Effect of (a) R, (b) Sr on rate of mass transfer

The comparison of rate of heat and mass transfer coefficients for different values of Eckert number (*Ec*) are shown in the Fig. 12.

From this figure, we noticed that the curves for rate of heat and mass transfer coefficients are close to each other. This means that, the numerical values of these coefficients are almost concur each other.

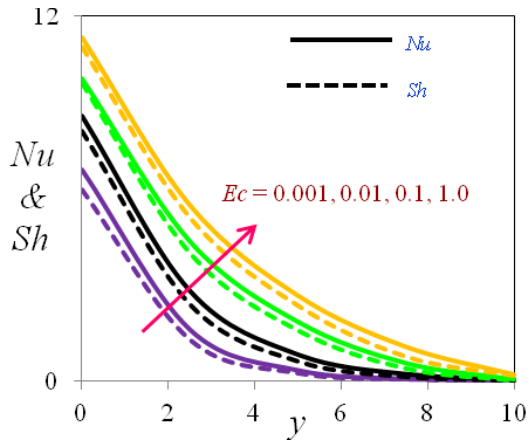

FIGURE 12. Comparison of rate of heat and mass transfer coefficients for different values of *Ec*

6. SUMMARY AND CONCLUSIONS

In the current study, the flow of an unsteady magnetohydrodynamic free convection past an infinite vertical plate in a porous medium under the synchronized effects of thermal-diffusion, diffusion-thermo, viscous dissipation and radiation is exaggerated by the stuff parameters. The governing equations are estimated to a system of linear partial differential equations by using finite element method. The results are opened graphically and we can conclude that the flow field and the quantities of physical awareness are significantly influenced by these parameters.

(1) Larger viscous dissipative heat causes an increase in the temperature plus the velocity profiles.
(2) As thermal radiation parameter increases, then there is a rise in both velocity and temperature profiles.
(3) The numerical results designate that the velocity increases with the increase in Grashof number for heat transfer and mass transfer, Darcy parameter, while it decreases as the magnetic field parameter, Prandtl number and Schmidt number increases.
(4) Dufour effects deeply influence the temperature profiles in the thermal boundary layer i.e. temperature profiles increases with the increase in the Dufour number.
(5) Soret effects are to enhance the concentration distribution with formation of concentration peak for superior values of Soret parameter in the concentration boundary layer.
(6) The numerical results obtained and compared with formerly reported cases available in the open literature and they are found to be in very good concurrence.

The analysis has shown that the temperature and concentration fields are appreciably predisposed by the Dufour and Soret effects. Thus we conclude that for some kind of mixture (i.e., H_2, *Air*) with the light molecular weight, the Soret and Dufour effects play an important role and should be considered in future studies.

NOMENCLATURE

x'	Coordinate axis along the plate (m)	x	Dimensionless Coordinate axis along the plate (m)
Sh	Sherwood number		
y'	Coordinate axis normal to the plate (m)	y	Dimensionless Coordinate axis normal to the plate (m)
B	Planck's function		
t'	Dimensional time (s)	t	Dimensionless time (s)
u'	Velocity component in x'-direct. (ms^{-1})	u	Dimensionless Velocity (ms^{-1})
w'	Velocity component in y'-direct. (ms^{-1})	H_0'	Transverse magnetic field ($tesla$)
g	Acceleration due to gravity (ms^{-2})	Sc	Schmidt number
T'	Fluid temperature ($^\circ C$)	T_w'	Fluid temperature at the wall ($^\circ C$)
T_∞'	Fluid temperature at free stream ($^\circ C$)	C'	Fluid Concentration (Kgm^{-3})
C_w'	Concentration at the wall ($Kg\ m^{-3}$)	Du	Dufour number
c_P	Specific heat at constant pressure	D	Solute mass diffusivity (m^2s^{-1})
P	Pressure (Nm^{-2})	Sr	Soret number
U_o	Dimensionless plate velocity (ms^{-1})	U	Free stream velocity (ms^{-1})
w_o'	Dimensional suction velocity (ms^{-1})	D_m	Molecular diffusivity (m^2s^{-1})
c_S	Concentration susceptibility ($mmole^{-1}$)	q'	Radiative heat flux (Wm^{-2})
M	Hartmann number	Pr	Prandtl number
Gr	Grashof number for heat transfer	Gc	Grashof number for mass transfer
K'	Dimensional porosity parameter (m^2)	O	Origin
C_∞'	Concentration at free stream (Kgm^{-3})	Ec	Eckert number
R	Thermal Radiation parameter	k_T	Mean absorption coefficient
C_f	Skin-friction Coefficient (Nm^{-2})	T_m	Mean fluid temperature
U'	Dimensional free stream velocity (ms^{-1})	A	Small positive parameter
Nu	Rate of heat transfer (or) Nusselt number	$K_{\lambda w}$	Mean Absorption coefficient

GREEK SYMBOLS

β	Coefficient of thermal expansion (K^{-1})	ρ	Fluid density (Kgm^{-3})
ε	Small positive parameter	v	Kinematic viscosity (m^2s^{-1})
τ'_w	Shear stress (Nm^{-2})	θ	Dimensionless temperature ($^\circ C$)
φ	Dimensionless concentration (Kgm^{-3})	ω'	Free stream frequency of oscillation
χ	Darcy number (Kd^{-2})	μ_e	Magnetic Permeability (Hm^{-1})
δ	Radiation absorption coefficient (cm^3s^{-1})	σ^*	Stefan-Boltzmann constant
κ	Thermal conductivity ($Wm^{-1}K^{-1}$)	ω	Dimensionless free stream frequency of oscillation (s^{-1})
σ_C	Electrical conductivity (Sm^{-1})		
β^*	Coefficient of Compositional expansion		
	Superscript		
$'$	Differentiation w.r.t. to y		
	Subscripts		
w	Wall condition	∞	Free stream condition

REFERENCES

[1] D. A. Nield and A. Bejan, *Convection in porous media*, Springer, NewYork, 2006.

[2] F. Garoosi, G. Bagheri and M.M. Rashidi, *Two phase simulation of natural convection and mixed convection of the nanofluid in a square cavity*, Powder Technology, **275** (2015), 239–256.

[3] F. Garoosi, L. Jahanshaloo, M.M. Rashidi, A. Badakhsh and M.A. Ali, *Numerical Simulation of Natural Convection of the Nanofluid in Heat Exchangers using a Buongiorno Model*, Applied Mathematics and Computation, **254** (2015) 183–203.

[4] M.M. Rashidi, B. Rostami, N. Freidoonimehr and S. Abbasbandy, *Free convective heat and mass transfer for MHD fluid flow over a permeable vertical stretching sheet in the presence of the radiation and buoyancy effects*, Ain Shams Engineering Journal, **5** (2014), 901–912.

[5] M. Sheikholeslami, M.M. Rashidi and D.D. Ganji, *Numerical investigation of magnetic nanofluid forced convective heat transfer in existence of variable magnetic field using two phase model*, Journal of Molecular Liquids, **212** (2015), 117–126.

[6] M.M. Rashidi, M. Ferdows, A. Basiri Parsa and S. Abelman, *MHD Natural Convection with Convective Surface Boundary Condition over a flat plate*, Abstract in Applied Analysis, 2014 (2014), Article ID 923487, 10 pages.

[7] M.M. Rashidi, T. Hayat, M. Keimanesh and A.A. Hendi, *New Analytical Method for the Study of Natural Convection Flow of a Non-Newtonian*, International Journal of Numerical Methods for Heat and Fluid Flow, **23** (2013) 436–450.

[8] Kang Cao and John Baker, *Non-continuum effects on natural convection-radiation boundary layer flow from a heated vertical plate*, International Journal of Heat and Mass Transfer, **90** (2015), 26–33.

[9] A. Andreozzi and O. Manca, *Radiation effects on natural convection in a vertical channel with an auxiliary plate*, International Journal of Thermal Sciences, **97** (2015), 41–55.

[10] S.O. Adesanya, E.O. Oluwadare, J.A. Falade and O.D. Makinde, *Hydromagnetic natural convection flow between vertical parallel plates with time-periodic boundary conditions*, Journal of Magnetism and Magnetic Materials, **396** (2015), 295–303.

[11] S. Sivaiah and R. Srinivasa Raju, *Finite element solution of heat and mass transfer flow with Hall current heat source and viscous dissipation*, Applied Mathematics and Mechanics (English Edition), **34** (2013), 559–570.

[12] B. Ganga, S. Mohamed Yusuff Ansari, N. Vishnu Ganesh and A.K. Abdul Hakeem, *MHD radiative boundary layer flow of nanofluid past a vertical plate with internal heat generation/absorption, viscous and Ohmic dissipation effects*, Journal of Nigerian Mathematical Society, **34** (2015), 181–194.

[13] V. Ramachandra Prasad and N. Bhaskar Reddy, *Radiation and mass transfer effects on an unsteady MHD free convection flow past a heated vertical plate in a porous medium with viscous dissipation*, Theoretical and Applied Mechanics, **34** (2007), 135–160.

[14] M.S. Dada and A.B. Disu, *Heat transfer with radiation and temperature dependent heat source in MHD free convection flow in a porous medium between two vertical wavy walls*, Journal of Nigerian Mathematical Society, **34** (2015), 200–215.

[15] Nabil T.M. Eldabe, Sallam N. Sallam and Mohamed Y. Abou-zeid, *Numerical study of viscous dissipation effect on free convection heat and mass transfer of MHD non-Newtonian fluid flow through a porous medium*, Journal of Egyptian Mathematical Society, **20** (2012), 139–151.

[16] Md. Ziaul Haque, Md. Mahmud Alam, M. Ferdows and A. Postelnicu, *Micropolar fluid behaviors on steady MHD free convection and mass transfer flow with constant heat and mass fluxes, joule heating and viscous dissipation*, Journal of King Saud University-Engineering Science, **24** (2012), 71–84.

[17] Dulal Pal, Babulal Talukdar, *Combined effects of Joule heating and chemical reaction on unsteady magnetohydrodynamic mixed convection of a viscous dissipating fluid over a vertical plate in porous media with thermal radiation*, Mathematics and Computer Modelling, **54** (2011), 3016–3036.

[18] H. Dessie and N. Kishan, *MHD effects on heat transfer over stretching sheet embedded in porous medium with variable viscosity, viscous dissipation and heat source/sink*, Ain Shams Engineering Journal, **5** (2014), 967–977.

[19] K.V. S. Raju, T. Sudhakar Reddy, M. C. Raju, P. V. Satya Narayana and S. Venkataramana, *MHD convective flow through porous medium in a horizontal channel with insulated and impermeable bottom wall in the presence of viscous dissipation and Joule heating*, Ain Shams Engineering Journal, **5** (2014), 543–551.

[20] M. Gnaneswara Reddy, Influence of thermal radiation, viscous dissipation and Hall current on MHD convection flow over a stretched vertical flat plate, Ain Shams Engineering Journal, **5** (2014), 169–175.

[21] E.R.G. Eckeret and R.M. Drake, *Analysis of heat and mass transfer*, McGraw Hill, New York, (1972).

[22] Siva Reddy Sheri and R. Srinivasa Raju, *Soret effect on unsteady MHD free convective flow past a semi-infinite vertical plate in the presence viscous dissipation*, International Journal of Computational Methods in Engineering Science and Mechanics, **16** (2015), 132–141.

[23] R. Srinivasa Raju, K. Sudhakar and M. Rangamma, *The effects of thermal radiation and Heat source on an unsteady MHD free convection flow past an infinite vertical plate with thermal diffusion and diffusion thermo*, Journal of Institution of Engineers: Series C, **94** (2013), 175–186.

[24] M.M. Rashidi and E. Erfani, *Analytical method for solving steady MHD convective and slip flow due to a rotating disk with viscous dissipation and Ohmic heating*, Engineering Computations, **29** (2012), 562–579.

[25] M.M. Rashidi, M. Ali, B. Rostami, P. Rostami and G.N. Xie, *Heat and Mass transfer for MHD viscoelastic fluid flow over a vertical stretching sheet with considering Soret and Dufour effects*, Mathematics Problems in Engineering, **2015** (2014), 1–12.

[26] M.M. Rashidi, T. Hayat, E. Erfani, S.A.M. Pour and A.A. Hendi, *Simultaneous effects of partial slip and thermal-diffusion and diffusion-thermo on steady MHD convective flow due to a rotating disk*, Communications in Nonlinear Science and Numerical Simulation, **16** (2011), 4303–4317.

[27] D. Srinivasacharya and Ch. RamReddy, *Soret and Dufour effects on mixed convection in a Non-Darcy Micropolar Fluid*, International Journal of Nonlinear Science, **11** (2011), 246–255.

[28] Gh.R. Kefayati, *FDLBM simulation of entropy generation in double diffusive natural convection of power-law fluids in an enclosure with Soret and Dufour effects*, International Journal of Heat and Mass Transfer, **89** (2015), 267–290.

[29] A.C. Cogley, W.G. Vincenti and S.E.Gill, *Differential approximation for radiative transfer in a non-gray-gas near equilibrium*, AIAA Journal, **6** (1968), 551–553.

[30] R. Bhargava and P. Rana, *Finite element solution to mixed convection in MHD flow of micropolar fluid along a moving vertical cylinder with variable conductivity*, International Journal of Applied Mathematics and Mechanics, **7** (2011), 29–51.
[31] Y-Y. Lin and S-P. Lo, *Finite element modeling for chemical mechanical polishing process under different back pressures*, J. Mat. Proc. Tech., **140** (2003), 646–652.
[32] W. Dettmer and D. Peric, *A computational framework for fluid-rigid body interaction: finite element formulation and applications*, Computational Methods in Mathematics and Applied Mechanics and Engineering, **195** (2006), 1633–1666.
[33] A. Hansbo and P. Hansbo, *A finite element method for the simulation of strong and weak discontinuities in solid mechanics*. Comp. Meth. Appl. Mech. Engg., **193** (2004), 3523–3540.
[34] K. J. Bathe, *Finite Element Procedures*, Prentice-Hall, New Jersy (1996).
[35] J. N. Reddy, *An Introduction to the Finite Element Method*, McGraw-Hill, New York (1985).